Journal of the European Ceramic Society **9** (1992) 309–322

Inherent Reinforcement of Ceramic Microstructures by Grain Boundary Engineering

A. Krell & P. Blank

Fraunhofer-Einrichtung für Keramische Technologien und Sinterwerkstoffe
(previously the Zentralinstitut für Festkörperphysik und Werkstofforschung),
Winterbergstr. 28, O-8020 Dresden, FRG

(Received 3 June 1991; revised version received and accepted 28 August 1991)

Abstract

Experiments with Al_2O_3/TiC (ATC) and with tetragonal $ZrO_2(Y_2O_3)/Al_2O_3$ (TZP-A) reveal a basically different distribution of amorphous phase at the grain boundaries. However, in both types of ceramic, the grain facets are free of flaws like micropores (which are typically observed in sintered aluminas) and are, hence, characterized by a high grain boundary toughness. On the other hand, the macroscopic toughness of TZP-A is in the same range as that of transformation-free ATC ceramics, because transformation toughening, though being the one important dissipation process in TZP-A, makes rather a small contribution. Therefore the comparison of materials with different grain boundary structures and toughening mechanisms like ATC and TZP-A gives rise to the idea that their high strength is not achieved by an enhanced macroscopic toughness but by an inherent reinforcement of their microstructures, resulting in an increased grain boundary toughness which provides a similar strength-improving mechanism independent of dissipative processes: limitation of the usual subcritical growth of extrinsic flaws due to the improved perfection of grain boundary structures.

Experimente mit Al_2O_3/TiC (ATC) und mit tetragonalem $ZrO_2(Y_2O_3)/Al_2O_3$ (TZP-A) zeigen eine grundlegend verschiedene Verteilung der amorphen Phase an den Korngrenzen. In beiden Keramiktypen sind die Kornfacetten frei von Fehlern wie Mikroporen (die aber typischerweise in gesintertem Aluminiumoxid beobachtet werden). Diese Werkstoffe sind daher durch eine hohe Zähigkeit der Korngrenzenbereiche gekennzeichnet. Andererseits aber liegt die makroskopische Zähigkeit von TZP-A in der gleichen Größenordnung wie die makropische Zähigkeit von unwandlungsfreien ATC-Keramiken, da die umwandlungsbedingte Zähigkeitssteigerung nur einen verhältnismäßig geringen Beitrag liefert, obgleich sie den wichtigsten Dissipations-Vorgang in TZP-A darstellt. Der Vergleich von Werkstoffen mit unterschiedlichen Korngrenzenstrukturen und zähigkeitssteigernden Mechanismen, wie der Vergleich von ATC und TZP-A, führt daher zu dem Gedanken, daß die hohe Festigkeit dieser Werkstoffe nicht aufgrund einer verbesserten makroskopischen Zähigkeit erreicht wird, sondern durch eine inhärente Verstärkung ihrer Gefüge entsteht, die zu einer gesteigerten Zähigkeit der Korngrenzenbereiche führt, die ihrerseits einen ähnlichen festigkeitssteigernden Mechanismus darstellt, der unabhängig von dissipativen Vorgängen ist: die Begrenzung des üblichen unterkritischen Wachstums von extrinsischen Fehlern infolge der erhöhten Perfektion der Korngrenzenstruktur.

Des expériences menées conjointement sur Al_2O_3/TiC (ATC) et sur de la zircone tétragonale $ZrO_2(Y_2O_3)/Al_2O_3$ (TZP-A) mettent en évidence une distribution radicalement différente de la phase amorphe aux joints de grain. Cependant, dans les deux types de céramiques, les facettes de grain sont exemptes de défauts tels que des micropores (qui sont typiquement observés dans les alumines frittées) et sont, en conséquence, caractérisées par une ténacité élevée des joints de grain. Par ailleurs, la ténacité macroscopique de la céramique TZP-A est du même ordre que celle des céramiques ATC ne comportant pas de transformation, car le renforcement par transformation de phase, bien qu'étant le seul mécanisme de dissipation important dans TZP-A, représente une contribution plutôt faible. Donc, en comparant des matériaux comme ATC et TZP-A, possédant des structures de joints de grain et des mécanismes de renforcement différents, on arrive à la conclusion que leur résistance mécanique élevée n'est pas due à une ténacité

Journal of the European Ceramic Society 0955-2219/92/$5.00

macroscopique améliorée, mais à un renforcement intrinsèque de leurs microstructures, dont découle une ténacité des joints de grain améliorée qui fournit un mécanisme similaire d'augmentation de la résistance indépendent des processus dissipatifs: la limitation de la croissance subcritique habituelle des défants extrinsèques, due à l'amélioration des structures de joint de grain.

Notation

$2a_0 + s$	Average size of flaws at triple-point junctions (existing as voids or filled with glass) plus standard deviation
$C_{m\text{-}ZrO_2}$	Concentration of monoclinic ZrO_2 related to the whole structure ($= X_m$ multiplied by the volume contents of ZrO_2)
$\bar{D}, D_{max}$	Average (linear intercept technique) and maximum grain sizes in sintered structures
E, E_0	Young's modulus (E_0: theoretical value of damage-free structures)
f^{Δ}	Frequency of triple-point flaws (voids or filled with glass)
f^{Δ}_{rel}	f^{Δ} related to the frequency of all triple-point junctions (completely and incompletely sintered)
G_c	Macroscopic critical energy release rate
K_{Ic}	Macroscopic toughness of polycrystalline structures (samples), measured by different methods:
K_{Ic}^{ISB}	Indentation strength in bending
K_{Ic}^{SENB}	Single-edge notched beam (notch width here 0·1 mm prepared before sintering to avoid preparation-induced martensitic transformation)
K_{Ic}^{L}	Fracture toughness of monocrystalline bulk material (crystal lattice)
K_{Ic}^{gb}	Critical stress intensity (toughness) of a fracturing grain boundary (depending on the microstructure of the interfaces between two grains)
PIF	Percentage of intercrystalline fracture along a crack path
ΔT	Temperature difference used to calculate strains resulting from thermal misfit
V_m	$= C_{m\text{-}ZrO_2} + \Delta C_{m\text{-}ZrO_2}$
X_m	Spontaneously generated monoclinic contents (related to the ZrO_2 phases only), measured by X-ray technique
ΔX_m, $\Delta C_{m\text{-}ZrO_2}$	Stress-induced increase in X_m, $C_{m\text{-}ZrO_2}$ on fracture surfaces
$\bar{\alpha}_{ZrO_2}$, $\bar{\alpha}_{Al_2O_3}$	Average coefficients of thermal expansion in ZrO_2, Al_2O_3
$\Gamma^0 (K_{Ic}^0)$	Macroscopic fracture energy (fracture toughness) of a microcrack-free structure without contributions of energy dissipative processes
Γ^{gb}	Fracture energy of a grain boundary
$\varepsilon_{t/m}$	Transformation strain
ν	Poisson's ratio
ρ, ρ_{th}	Density of sintered structures (ρ_{th} = theoretical value)
ρ_{mc}	Density of microcracks that intersect the macroscopic fracture surface of a sample
σ_f	Macroscopically measured fracture strength of polycrystalline samples
σ_f^{gb}	Grain boundary strength ($\sim K_{Ic}^{gb}/\sqrt{a_0}$ or $\sim K_{Ic}^{gb}/(2a_0 + s)^{1/2}$)
$\sigma_1(r)$	Localized at some stress concentrator microscopic stress field
σ_{pc}	Initiation stress for martensitic transformation
σ_{res}^1	Effective residual tension stress due to (i) thermal misfit and thermal expansion anisotropy, and (ii) visco-elastic relaxation
ω	Damage parameter ($= (2/9)\rho_{mc}$)

1 Introduction

Well-known concepts treating grain boundary energies (Γ^{gb}) in metals[1] and ceramics[2] can be related to stress intensity (K_{Ic}) formulations by inserting Γ^{gb} instead of Γ into the general relationship $K_{Ic} = [2E\Gamma/(1-\nu^2)]^{1/2}$ where E is Young's modulus and ν is Poisson's ratio. A measuring method for the critical stress intensity K_{Ic} that characterizes the toughness of plain macroscopic interfaces has been proposed by Suga & Elssner.[3] Similarly, the microscopic equivalent is the interface between two grains, the grain boundary, which can be described by a grain boundary toughness K_{Ic}^{gb}.[4]

Hence, just as on the macroscopic scale, the grain boundary strength depends on K_{Ic}^{gb} and on the size of flaws existing adjacent to the fracturing interface (e.g. small pores at the position of triple-point junctions). Grain boundary structures with improved microscopic K_{Ic}^{gb} should be able to raise both the macroscopic (sample) toughness at crack instability and the resistance against subcritical crack growth. The latter reduces the finally developed critical flaw size and may result in an increase of

strength which is more pronounced than that of the toughness K_{Ic}.[5]

Different grain boundary toughnesses have been measured depending on doping concentrations[4] and on sintering atmosphere,[6] and are observed to be associated with the occurrence of amorphous grain boundary films. For aluminas sintered with and without additions of unstabilized zirconia it has been demonstrated by high-resolution TEM that grain boundaries containing amorphous phases coexist with entirely glass-free interfaces;[7] even if a triple-point junction is completely filled with glass the amorphous phase frequently does not enter the adjacent boundaries. The frequency of amorphous interfaces in such structures is increased by powder processing technologies that enhance the glass concentration—an effect that is often accompanied by a decrease in the grain boundary toughness.

This decrease should be the more pronounced if the occurrence of amorphous films favours the development of micropores within the flat boundary facets as observed previously.[4] Figure 1 presents an example of a replica TEM micrograph showing the fracture surface of hydrogen-sintered alumina doped with 0·15 wt% MgO and 0·06 wt% Pb, and containing an impurity level of about 0·3 wt% SiO_2. Clearly most of the grain surfaces are decorated by a lot of micropores with a size of 50–150 nm. Any misinterpretation of these features as random artefacts is excluded by the existence of plain and almost defect-free transcrystalline fracture areas. Nonstationary nucleation[8] and growth of such microporosity have been discussed as being promoted by

(i) high residual microstresses,
(ii) low microviscosity or high diffusion constants within the interfaces,[9] and
(iii) sufficiently long time periods of cooling through the temperature interval corresponding to rigid grains but deformable interface regions.[10]

The three conditions together are required to generate grain boundary microporosity which, therefore, can be suppressed by avoiding just one of them. For example, rapid cooling is observed to increase the strength, σ_f, of sintered alumina at almost unchanged residual stress due to a mechanism of kind (iii).[11] The same examinations have revealed lower residual stresses in alumina sintered in air than after sintering in hydrogen, and it is just the air-sintered ceramic that exhibits an especially low micropore density according to mechanism (i) and associated with the highest K_{Ic}^{gb}.[6]

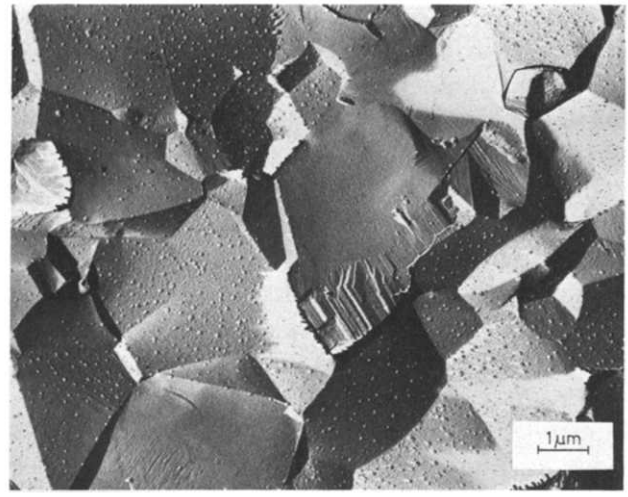

Fig. 1. C/Pt replica micrograph of the fracture surface of hydrogen-sintered alumina doped with 0·15 wt% MgO/0·06 wt% PbO and with an impurity content of 0·3 wt% SiO_2. Micropores are visible on most of the grain surfaces (before fracture: grain boundaries).

In addition to amorphous phases and micropores, the spatial and size distribution of incompletely sintered triple-point junctions is a third feature expected to affect the micromechanical performance. A favourable, if only indirect, influence of decreasing grain sizes can then emerge from at least two processes: the size of triple-point pores decreases (at constant sample density) with the grain size and, during the cooling of the sintered structures, the smaller grain sizes bring about an intense relaxation of developing residual stresses, thus hindering the generation of microporosity.

The present study was intended to establish whether, in ceramics with median macroscopic toughness K_{Ic}, technological measures based on mechanisms (i) and (ii) to suppress grain boundary microporosity would be able to enhance the strength, e.g. by reducing the subcritical growth of extrinsic flaws. To find an answer that is generally valid the question was addressed examining extremely different structures: as an example in the sense of mechanism (i) a transformation-free structure (Al_2O_3/TiC [ATC]) without any amorphous boundary phase was used, and submicron Y-TZP (tetragonal ZrO_2 stabilized with Y_2O_3) where all interfaces are covered with glass was tested with respect to mechanism (ii) To avoid misinterpretations caused by the mentioned extremely different grain boundary structures in ATC and in Y-TZP sintered alumina was included into the investigations as a second transformation-free material.

To evaluate the possibility of an increased strength due to improved grain boundary perfection and reduced subcritical growth Y-TZP will be

suitable only if its failure is not simply initiated by very small intrinsic (associated with the small grain size) Griffith flaws. Hence questions have to be asked about the character of the defects that initiate fracture in Y-TZP.

Recent attention has focused on Y-TZP as being the first pressureless sintered ceramic with a simple globular (equiaxed grain) microstructure and a bending strength of about 900–1300 MPa without reinforcement by fibres, whiskers or elongated grains.[12,13] The strength can be further increased by hot isostatic pressing and by adding 10–40 wt% alumina—although with 3 mol% Y_2O_3 the macroscopic K_{Ic} usually does not exceed 6 MPa$\sqrt{m}$.[14,15]

The fine ZrO_2 powder raw materials and the influence of 2–3 mol% Y_2O_3 additions[16] allow green bodies to be sintered to densities of 98–99% of the theoretical maximum at fairly low temperature, preserving small ZrO_2 grain sizes of about 0·4–0·8 μm. It has been argued by Hoshi *et al.*[17] that—additionally to an influence of K_{Ic} due to transformation toughening—the high strength is caused by the small grain size assumed by Wang *et al.*[18] to be associated with corresponding small (intrinsic) Griffith flaw sizes.

This interpretation is substantiated by experiments with single-phase, transformation-free alumina ceramics: here, too, the strength is almost doubled (to about 700 MPa with conventional powder processing) when fine dispersed raw materials enable sintering to 99% density at low temperatures, resulting in small grain sizes of 0·8 μm.[17,19] Further, whereas the 'usual' strength of pressureless sintered alumina toughened with about 12 vol.% of unstabilized ZrO_2 (ZTA) is 600–700 MPa, there are examples of 1250–1400 MPa with an extremely narrow grain size range of 0·3–2·0 μm and with a toughness of only about 4·5 MPa$\sqrt{m}$.[20,21] Additionally, Shin *et al.*[22] have noticed improved strength in HIP-ZTA associated with a *decrease* in the stress-induced transformation—indicating a reduced influence of energy dissipation on the strength in the range above 900 MPa.

However, there is one strong argument against small intrinsic flaws proportional to the grain size acting as the main cause for such high strengths. It emerges from the mechanical data of just those high-strength–small grain size zirconias and aluminas that applying simple fracture mechanics gives the size of the critical flaw at instability $(K_{Ic}/\sigma_f)^2$ in the range between 10 μm (TZP) and 40 μm (Al_2O_3)—a fair order of magnitude more than the respective grain sizes but close to the usual sizes of extrinsic flaws produced due to technological shortcomings.

It is another objective of this study to give evidence about the extrinsic or intrinsic character of the flaws which are responsible for the fracture of fine-grained Y-TZP.

2 Materials and Methods

Fundamental data and processing parameters are documented in Table 1. Homogenization of the alumina/titanium carbide material (ATC) was achieved by attrition milling in water for 40 min with 85% Al_2O_3 balls, whereas all other ceramics were prepared with a planetary ball mill. Different structures of tetragonal zirconia polycrystals (TZP) were fabricated with low (TZP–L: 0·2 wt%), medium (TZP–M: 0·5–0·6 wt%) and higher (TZP–H: 0·8 wt%) SiO_2 concentrations, divided into batches with coarse (index C) and with very fine-grained (index F) alumina additions; since all of the TZP structures investigated here contain some Al_2O_3, the index A used in the abstract is omitted. The coarse alumina grains, introduced to produce large flaws by differential sintering as described by Tuan & Brook,[23] have been generated using low-strength alumina milling balls of different impurity levels with coarse grains. Two TZP-MC structures with different Al_2O_3 grain size distributions had to be prepared to evaluate (i) the possible influence of rising SiO_2 concentration at constant grain size (LC–MC[a]) and (ii) the effect of different Al_2O_3 grain sizes at a constant SiO_2 content (MC[a]–MC[b]). All specimens were pressed uniaxially with 200 MPa from freeze-dried powders. The final dimensions of sintered bars were $6 \times 4 \times 50\,mm^3$.

For comparative purposes alumina and zirconia-toughened alumina (ZTA) ceramics were prepared by basically the same technology as that used for TZP but with addition of 0·15 wt% MgO and 0·06 wt% PbO to prevent exaggerated grain growth and to yield small concentrations of a low viscosity grain boundary glass phase. A range of technological measures was used for the production of the well-known standard materials to get a general idea about the performance independent of one special technology. Therefore, for Al_2O_3 and ZTA, Tables 1 and 2 give some ranges for the evaluated parameters arising from, for example, different sintering atmospheres or different raw materials for the ZrO_2 addition.

Sintering conditions were varied in a first step. For example, for TZP the tested range of parameters was constant heating rates between 1 and 100 K/min, temperatures 1250–1600°C and isothermal hold

Table 1. Fundamental data for the examined materials: raw materials, optimum sintering conditions used and most important parameters characterizing the resulting sintered structures

	Al_2O_3	*ATC*	*ZTA*	*TZP-LC*	*TZP-MC[a]*	*TZP-MC[b]*	*TZP-HF*
Composition (wt%)	Al_2O_3 +0·15 MgO +0·06 PbO +0·2–0·4 SiO_2	Al_2O_3 +40 TiC +0·5 SiO_2	Al_2O_3 +17 ZrO_2 +0·15 MgO +0·06 PbO +0·2–0·4 SiO_2	$ZrO_2(Y_2O_3)$ +16 Al_2O_3 +0·15 SiO_2	$ZrO_2(Y_2O_3)$ +28 Al_2O_3 +0·6 SiO_2	$ZrO_2(Y_2O_3)$ +25 Al_2O_3 +0·5 SiO_2	$ZrO_2(Y_2O_3)$ +6 Al_2O_3 +0·8 SiO_2
Basic raw materials	Alcoa A16SG	CT 3000SG + Starck TiC (c.a.s.)	Alcoa A16SG + Soviet ZrO_2 or $ZrOCl_2 \cdot 8H_2O$	Dynazirkon F-5Y			
Sintering conditions	1560–1600°C, 1–2·5 h, H_2 or air	1800°C, 3 h, Ar + HIP: 1400°C/2 h, Ar (100 MPa)	1500–1580°C, 1 h, H_2	1400°C, 6 h, air	1500°C, 2 h, air	1450°C, 4 h, air	1350°C, 4 h, air
ρ, g/cm³	3·92–3·94	4·23	4·14–4·18	5·52	5·15	5·28	5·93
ρ/ρ_{th}, %	98·3–98·8	98·3	98·0–98·9	98·4	98·8	99·0	100
$\bar{D}(D_{max})$, μm	2·5–3·0	Al_2O_3: 2·8 TiC: 1·8	Al_2O_3: 2·2 ZrO_2: 1·1	ZrO_2: 0·6 Al_2O_3: 1·8 (8)	0·7 1·8 (7)	0·6 2·0 (20)	0·25 0·6 (2)
E, GPa	375–390	390	350–360	220	265	240	210
E/E_{th}	0·94–0·98	0·98	0·94	0·84	0·92	0·85	0·93
X_m	—	—	0·29	0·03	0·05	0·06	0·02
$C_{m\text{-}ZrO_2}$, vol.%	—	—	3·3	2·3	3·2	4·0	1·8
ΔX_m	—	—	+0·10	+0·14	+0·17	+0·10	+0·11
$\Delta C_{m\text{-}ZrO_2}$	—	—	1·2	11·2	10·7	6·6	10·0

Symbols used for TZP ceramics: L/M/H—low/median/high SiO_2 contents; C/F—coarse/fine-grained Al_2O_3 additions.

times 1–8 h. Since the objective of the work was not to study the effect of differing sintering conditions but to evaluate interdependences between microstructures and macroscopic properties as *generally typical* for the different materials, Tables 1 and 2 present sintering results for only those conditions that produced the highest strength for ATC and for TZP, respectively.

The density ρ was measured following Archimedes' principle, the average grain size $\bar{D}$ by the linear intercept technique. Young's modulus E was determined from the resonance frequency of bars,

Table 2. Quantitative results of structural observations and macroscopic mechanical parameters. The density of microcracks intersecting the fracture surface is ρ_{mc}. See text for parameters that characterize triple-point size and frequency

	Al_2O_3	*ATC*	*ZTA*	*TZP-LC*	*TZP-MC[a]*	*TZP-MC[b]*	*TZP-HF*
K_{Ic}^{gb}, MPa$\sqrt{m}$	1·4–1·8	2·3	(1·8)	—	—	($\approx$5)	—
K_{Ic}^{gb}/K_{Ic}^{L}	0·58–0·74	0·98	0·74	—	—	$\approx$1	—
σ_f^{gb}, GPa	1·6–2·1	4·0	(2·8)		—	20–35	—
$2a_0 \pm s$, μm	0·6 ± 0·40 −0·69 ± 0·55	0·31 ± 0·20	0·35 ± 0·32			0·05 ± 0·05	
f^A, $\times 10^9$ m^{-2}	21–47	38	79			300	
f_{rel}^A	0·153–0·343	0·224	0·185			0·075	
ρ_{mc}	0·73–1·16	0·75	1·8			1·4	
K_{Ic}^{ISB}, MPa$\sqrt{m}$	3·7–3·9	4·8	—	—	—	—	—
K_{Ic}^{SENB}, MPa$\sqrt{m}$	3·5–3·9	—	5·3–6·3	4·4	4·3	5·4	4·3
σ_f, MPa							
20°C	400 ± 30 −460 ± 40	Sintered: 664 ± 18 + HIP: 753 ± 14	600 ± 55 −665 ± 35	974 ± 13	731 ± 17	942 ± 72	689 ± 53
1000°C	—	738 ± 84	370 ± 45	—	—	392 ± 12	—

Calculated results for K_{Ic}^{gb} and σ_f^{gb} are given in parentheses.

and the monoclinic amount of ZrO_2, X_m (related to all ZrO_2 phases), was assessed from monoclinic, tetragonal and cubic (111) reflections using Co-K_α X-rays. From the volume contents of all ZrO_2 phases the concentration of monoclinic ZrO_2, $C_{m\text{-}ZrO_2}$ (related to the whole sintered structure), was derived.

The occurrence of monoclinic ZrO_2 in unstressed structures was due to the spontaneous martensitic transformation of originally tetragonal zirconia grains during cooling of sintered specimens. High residual stresses are then generated,[24] which, depending on $C_{m\text{-}ZrO_2}$ and matrix properties, may or may not provoke spontaneous microcracking.[25] Since this kind of microdamage is reflected in the elastic behaviour but not in the relative density (ρ/ρ_{th}), Table 1 includes (E/E_{th}) for all the examined materials.

The grain boundary toughness K_{Ic}^{gb} was estimated, as has been introduced previously.[4] The basic idea is that under conditions of slow, quasi-static crack growth the ratio of K_{Ic}^{gb} to the lattice value K_{Ic}^{L} will determine the percentage of intergranular fracture (PIF, related to the whole inter- and transgranular fracture path):

$$K_{Ic}^{gb}/K_{Ic}^{L} = f(\text{PIF}) \qquad (1)$$

It had been shown that in a two-dimensional analysis the functional dependence f(PIF) is the same one as that of $f(\alpha)$ describing the decrease of the stress intensity K_I at some inclination α of the crack plane against the tension stress. Whereas in a first treatment the relation for a crack inclined as a whole, $K_I(\alpha) = f(\alpha) = \cos^2\alpha$, had been used, it was understood that this $f(\alpha)$ would become increasingly incorrect at large PIF:[6] when studying the behaviour of the tip of a slowly propagating crack, it is more realistic to address the crack as a straight one with a short inclined tip, e.g. just circumventing a grain. An elaborated analysis of the problem gives a weaker dependence on α than $\cos^2\alpha$; this has been graphically represented by Cotterell & Rice[26] and is reproduced in Fig. 2. This $f(\alpha)$ is used here to calculate $K_{Ic}^{gb}/K_{Ic}^{L} = f$(PIF).

TEM micrographs were used to measure the average size $2a_0$ of triple-point flaws (voids or glass-filed pores), the standard deviations s of this parameter and the frequency f^{Δ} of these microscopic stress concentrators. Related to the frequency of all of the triple-point junctions (completely sintered, incompletely sintered but free of glass, pores filled with glass), f_{rel}^{Δ} gives the relative density of that kind of flaws.

C–Pt replicas were prepared from fracture surfaces for two purposes. Firstly, replication was used

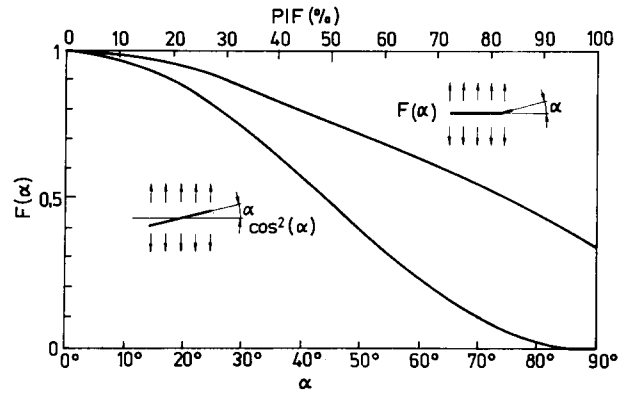

Fig. 2. Angular dependence of the crack tip stress intensity K_I for an inclined crack and for a crack perpendicular to stress with an inclined tip of infintesimal length,[26] used to determine the ratio K_{Ic}^{gb}/K_{Ic}^{L} of the critical stress intensities of grain boundary and crystal lattice.

to reveal microcracks which intersect the fracture surface, and a quantitative determination of this crack density, ρ_{mc}, can be performed.[25,27] Secondly, tiny micropores as shown by Fig. 1 usually are very flat, lens shaped and, therefore, extremely difficult to identify by high-resolution TEM but are well reproduced by replica micrographs.

The macroscopic fracture toughness K_{Ic} of the transformation-free ceramics was determined by measuring the indentation strength in bending (ISB) at a Vickers load of 10 kg.[28] The basic presupposition of this method is that the ratio of the indent size to the produced crack length is describable by the ratio of elasticity to hardness without influence from other factors that do not affect E/H.[29] Hence erroneous results may be produced when applying this ISB technique to materials with *different* degrees of load-induced phase transformations and, therefore, varying residual stresses. For example, Hecht *et al.*[20] found significant differences up to 150% for a variety of ZTA, Mg-PSZ, Ce-TZP and Y-TZP materials when comparing K_{Ic} measured by controlled flaw and by microindentation methods, respectively. Therefore a single-edge notch beam method (SENB) has been proposed in which a 0·1 mm narrow notch is produced before sintering, avoiding any additional transformation of ZrO_2 grains on notching or reannealing sintered structures.[25] This method has been used here for Al_2O_3 (for comparative purposes), for ZTA and for all kinds of TZP materials. As a previous test, both the ISB and the SENB techniques were applied for sintered, 98·5% dense Al_2O_3 with an average grain size of 2·5 μm, and the results were almost identical: $K_{Ic}^{ISB} = 3{\cdot}7\text{–}3{\cdot}9\ \text{MPa}\sqrt{\text{m}}$, $K_{Ic}^{SENB} = 3{\cdot}5\text{–}3{\cdot}9\ \text{MPa}\sqrt{\text{m}}$.

All K_{Ic} and strength data were obtained in three-point bending tests with a cross-head velocity of 0·5

(strength) and 1 mm/min (K_{Ic}). The span was 25 mm for K_{Ic}, 30 mm for room-temperature strength testing and 40 mm when measuring at 1000°C in a vacuum. Al_2O_3 and ZTA specimens were tested in the as-sintered state, whereas ATC and Y-TZP samples were ground with a resin-bonded 40–50 μm diamond wheel—a treatment that avoided grinding-induced transformation and resulting residual stress influences on the strength.

3 Experimental Results

3.1 Structural observations

General characteristics of the examined ceramics are concentrated in Table 1. In contrast to hydrogen-sintered Al_2O_3 (Fig. 1) and ZTA, fewer grain boundary micropores were detected in air-sintered alumina at the same doping and impurity level, and almost no such pores were observed in ATC (Fig. 3(a)) and in TZP (Fig. 3(b)) in spite of the basically different distributions of glass phases in the boundary regions of those latter materials. TEM analyses revealed the following features (for high-resolution TEM micrographs see Refs 7 and 30).

—In ATC all of the grain boundary facets are free of any amorphous films or thin crystalline third-phase layers. About 1/5 of all of the triple-point junctions are incompletely sintered (f_{rel}^{Δ} in Table 2), existing almost exclusively as glass-free voids.

—In both Al_2O_3 and ZTA the typical situation is a coexistence of neighbouring grain facets with and without glassy interfaces. The frequency of incompletely sintered triple points, most of them being glass-free pores, is about the same in Al_2O_3 and ZTA as in ATC. Their size, however, is doubled in alumina with respect to ZTA and ATC (Table 2).

—Only in TZP are all of the grain boundary facets covered with glass at a SiO_2 content of 0·2–0·5 wt%; the thickness of these amorphous films (about 0·6 nm) is somewhat less than in Al_2O_3 or in ZTA. The absolute frequency of triple-point flaws, almost all of them filled with glass in TZP, is very high because of the small grain size and the resulting large number of triple junctions per volume. On the other hand, their size is extremely small for the same reason, and their relative frequency is remarkably low.

In spite of the perfect microstructure of the TZP matrix with the lowest relative frequency and smallest size of (glass-filled) triple flaws and with

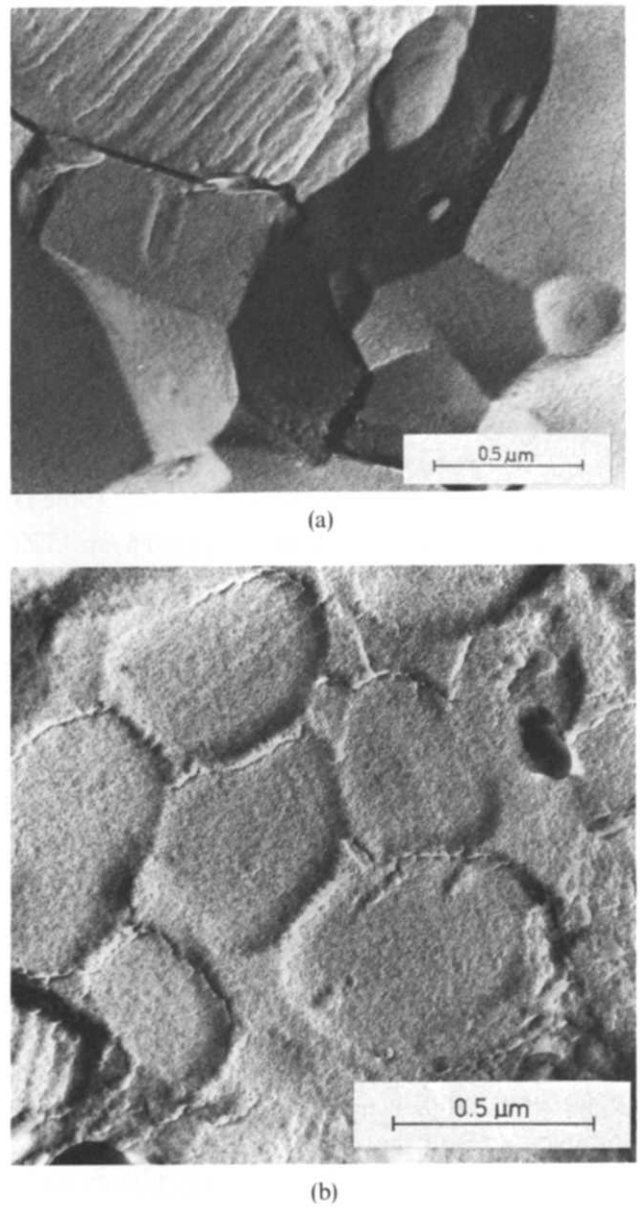

Fig. 3. C/Pt replica micrograph of micropore-free grain boundaries on fracture surfaces of (a) ATC (Al_2O_3/TiC with 0·5 wt% SiO_2) and (b) TZP–MC[b] (ZrO_2/3 mol% Y_2O_3 with 25 wt% of coarse-grained Al_2O_3 and 0·5 wt% SiO_2).

interfaces that are free of microporosity, the amount of unstably formed regions of intergranular fracture was found to be largest in TZP, as is typical for very fine-grained structures (≥90% in Al_2O_3 free sub-regions). It is much smaller (58%) in ATC, which is free of microporosity and of amorphous interfaces and has a larger grain size than Y-TZP. The crack density detected on fracture surfaces is lowest in ATC (0·75) and in air-sintered alumina (0·73) but is somewhat increased in H_2-sintered Al_2O_3 (1·16). It is on a median level in TZP (1·4) and highest in ZTA (1·8).

It has been suggested that the stress concentration at a propagating macrocrack provides local stresses which, close to the tip, are higher than any grain

boundary strength that has yet been measured in alumina, with the consequence that the generated microcrack density should not depend primarily on K_{Ic}^{gb} but on the local sizes and associated width of distribution of microflaws.[4] This idea agrees qualitatively with the results for transformation-free structures presented in Table 2: with similar residual stresses, the materials with the lowest triple pore frequency (air-sintered Al_2O_3: $f_{rel}^{\Delta} = 0{\cdot}153$) and the smallest pore size (ATC: 0·31 μm) exhibit the smallest microcrack densities of 0·73–0·75.

To ensure a low degree of *spontaneous* martensitic transformation (in Table 1 X_m relates to ZrO_2 and $C_{m\,ZrO_2}$ relates to the whole structure) it is sufficient to meet one of the following conditions (Table 1):

—low silica content at $\bar{D}(ZrO_2) \approx 0{\cdot}6\ \mu m$ (TZP-LC);

—reduced ZrO_2 grain size at an SiO_2 content of 0·5–1% (TZP-HF: 0·25 μm).

However, stress-induced transformation *on fracture* is obviously governed by other features: all of the examined TZP structures on fracture revealed the same $\Delta X_m \approx 0{\cdot}14 \pm 0{\cdot}04$.

3.2 Mechanical measurements

The result of crack path studies is exemplified by Fig. 4. The percentage of intergranular fracture was in the range of 55–75% for the various aluminas investigated, but only 12% for ATC. With eqn (1) and Fig. 2 these PIF give K_{Ic}^{gb}, as documented in Table 2. The grain boundary fracture toughness is about 40% higher in ATC than in pure Al_2O_3 ceramics, a result that agrees well with the observed absence of any glassy grain boundary phases and of interface pores in ATC. To calculate the absolute value given in Table 2 an averaged $K_{Ic}^{L} = 2{\cdot}35$ $MPa\sqrt{m}$ (according to the volume contents of Al_2O_3 and TiC) was used, based on the data $K_{Ic}^{L}(Al_2O_3) = 2{\cdot}5\ MPa\sqrt{m}$ and $K_{Ic}^{L}(TiC) = 2{\cdot}2$ $MPa\sqrt{m}$, as derived from various sources.[31–34]

Compared with Al_2O_3, the improvement by 40% in K_{Ic}^{gb} is associated, however, with an increase of the macroscopic K_{Ic} by only about 30%, whereas the strength is increased by 50% (sintered ATC) or even 75% (HIP-ATC), respectively. Hence there must be additional mechanisms that are responsible for the high room-temperature strength of ATC besides that of the macroscopic toughness. No significant change in the strength of ATC has been observed from room temperature up to 1000°C.

Crack propagation-induced martensitic transformation in ZrO_2-containing ceramics is demonstrated by ΔX_m and $\Delta C_{m\text{-}ZrO_2}$ in Table 2. Resulting

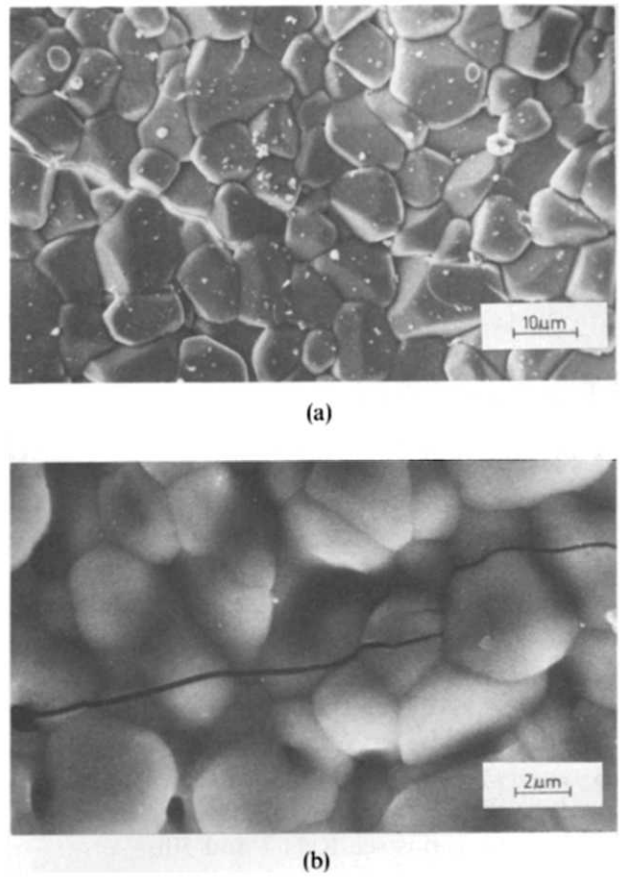

Fig. 4. Scanning electron micrographs showing radial cracks emanating from Vickers indentations: (a) crack tip in alumina (as-sintered surface); (b) crack in ATC (thermally etched surface). The percentage of intergranular fracture (PIF) was observed to be independent of the investigated location along the crack and unaffected by the used regime of thermal etching that, however, produced some surface porosity at 1400°C/2 h/Ar(CO). PIF is obviously smaller in ATC, representing an increased grain boundary toughness.

residual stresses might affect PIF and produce incorrectly calculated K_{Ic}^{gb} values. Therefore this method should not be used to evaluate the interface toughness of such materials. However, the microcrack density in ZTA can be compared with the various TZP structures listed in Table 2: in TZP ρ_{mc} is much lower in spite of a significantly enhanced $\Delta C_{m\,ZrO_2}$ and associated increased residual stresses acting on fracture. This is an indication of a raised K_{Ic}^{gb} in TZP (free of micropores (Fig. 3(b)) and containing a very low relative frequency of extremely small triple flaws). It turns out that under such circumstances microcracking is not promoted by amorphous grain boundary phases, the frequency of which is much higher in TZP than in ZTA. All this reasoning leads to the conclusion that an approximation, $K_{Ic}^{gb} \approx K_{Ic}^{L}$, should work for TZP just as has been measured for ATC. However, tetragonal ZrO_2 (3 mol% Y_2O_3) monocrystals show very high $K_{Ic}^{L} =$ 6–9 $MPa\sqrt{m}$.[35,36] Regarding the macroscopic

toughnesses of the investigated TZP materials in Table 2, $K_{Ic}^{gb} \approx K_{Ic}^{L} \approx 5\,MPa\sqrt{m}$ is assumed to be a realistic estimate.

There is no ready indication of transformation *toughening* in TZP: in comparison with ZTA significantly *enhanced* $\Delta C_{m\text{-}ZrO_2}$ are associated with *lower* K_{Ic} (Tables 1 and 2), and no correlation between K_{Ic} of different TZP and their $\Delta C_{m\text{-}ZrO_2}$ can be found.

Some influence of microcrack toughening might be suggested by the increase of the crack densities and of K_{Ic} in the pure oxidic materials ranking $Al_2O_3 < TZP < ZTA$ (Table 2). On the other hand, ATC has almost the same toughness as TZP but with a fairly low microcrack density. This, however, gives no bias against a microcrack mechanism as long as the effects of the different residual stresses and of K_{Ic}^{gb} are not considered (cf. Section 3.3). At higher temperatures the TZP–MC[b] exhibits a similar drop in strength, as observed with ZTA in spite of the high Al_2O_3 content of 25%.

3.3 Complementary calculations

In addition to the high K_{Ic}^{gb}, a further contribution to an increased grain boundary strength of TZP should result from the small size of microscopic stress concentrators. Since microfracture will be initiated by the larger of the flaws, it has been proposed to estimate the microstrength with

$$\sigma_f^{gb} = \sqrt{\pi}\, K_{Ic}^{gb} / \sqrt{2(2a_0 + s)} \qquad (2)$$

instead of using the average size $2a_0$.[4] For TZP this procedure would give a grain boundary strength of about 20 GPa in the presence of usual triple-point voids. In TZP, however, no such voids exist because all incompletely sintered triple junctions are filled with glass. The glass increases the triple-point/matrix ratio of Young's moduli from zero (for a pore) to about 0·3, and for aspect ratios of 0·5–2 this effect reduces the local stress to about 0·55 (Kreher, W., pers. commun., 1990). The consequence is a further increase of the effective σ_f^{gb} in TZP to about 35 GPa (Table 2), and the difference compared with other ceramics might become even greater when the low relative triple flaw frequency in TZP is considered. Because of very similar grain boundary structures K_{Ic}^{gb} in ZTA is expected to be on the same level as in Al_2O_3 with a somewhat higher microstrength due to smaller triple flaws.

As mentioned in Section 3.2, to evaluate the role of competing energy dissipative mechanisms the ratio of residual stresses to the critical stresses initiating microcracking (σ_f^{gb}) or phase transformations (σ_{pc}) must be incorporated, in addition to the degree of transformation $\Delta C_{m\text{-}ZrO_2}$ and the generated crack density ρ_{mc}. The model proposed by Kreher treats within one framework (I) microcrack dissipation of stored elastic strain energy in single-phase ceramics, (II) microcracking around transformed monoclinic ZrO_2 and (III) transformation toughening[37,38] (including wake effects). In Table 3 E_0 is the Young's modulus for undamaged structures (free of microcracks) and σ_f^{gb} and σ_{pc} are used as introduced previously (σ_{pc} is evaluated with a formula given by Ref. 39 and using experimental data for the size of transformation zones in ZTA and Y-TZP). The volume contents $\Delta C_{m\text{-}ZrO_2}$ of transforming ZrO_2 are taken from Table 1, and $V_m = C_{m\text{-}ZrO_2} + \Delta C_{m\text{-}ZrO_2}$ is the sum of the spontaneously generated and of the fracture-induced monoclinic contents. The linear strains from transformation and thermal misfit are estimated with commonly known data for $\Delta T = -1500$ K. The residual tension

Table 3. Comparison of the effects of (I) microcracking due to thermal mismatch (or expansion anisotropy), of (II) microcracking around transformed monoclinic ZrO_2 particles, and of (III) microcrack-free transformation toughening using the model of Kreher[38] with Poisson's ratio $\nu = 0{\cdot}2$

	Al_2O_3	ATC	ZTA			TZP–MC[b]	
E_0, GPa	400	400	360			215	
σ_f^{gb}, GPa	2	4	2·8			35	
σ_{pc}, MPa	—	—	1·3			1·7	
$\Delta C_{m\text{-}ZrO_2}$, vol.%	—	—	1·2			8·6	
V_m, vol.%	—	—	4·5			12·6	
$\varepsilon_{t\,m}$, %	—	—	1·4			1·4	
$(\bar{\alpha}_{ZrO_2} - \bar{\alpha}_{Al_2O_3})\Delta T$, %	—	—	−0·3			−0·3	
σ_{res}^{t}, MPa	60	60	Al_2O_3–matrix:60			≈0	
ω	0·16–0·26	0·17	0·40			0·31	
Dissipation mechanism	I	I	I	II	III	II	III
$G_c/2\Gamma^0(1-\omega)$	1·03–1·07	1·04	1·13	4·14	2·34	1·08	1·31
$G_c/2\Gamma^0$	0·87–0·97	0·86	0·68	2·48	1·40	0·75	0·90
K_{Ic}/K_{Ic}^0	≈1	≈1	—	1·6	—	—	≈1

stresses have been measured in Al_2O_3[11] and in ATC;[40] they are expected to be near zero in the fine-grained TZP due to its extended ability for relaxation. With the microcrack densities ρ_{mc} from Table 2 a damage parameter for arbitrary microcrack orientation is defined by $\omega = (2/9)\rho_{ms}$.

The resulting critical energy release rates are given in Table 3 for the three competing mechanisms related to the 'dissipation-free' toughness $2\Gamma^0$ (which becomes decreased by a factor $(1-\omega)$ due to microcrack damage). Since residual stresses should be small in Y-TZP, no calculation for microcrack dissipation associated with thermal expansion anisotropy (I) was performed for this material. G_c calculated for this mechanism (I) in ZTA assumes all microcracking to be associated with (I) only—which is certainly not true: since preferred cracking around monoclinic ZrO_2 grains is observed, energy will be dissipated first of all by process (II), and mechanism (I) must be overestimated in Table 3.

The following results are indicated by Table 3:

—For usual Al_2O_3 and ATC ceramics no significant enhancement of the toughness occurs due to microcracking around the crack tip or in the wake. The most probable explanation for the difference between the macroscopic K_{Ic} of alumina ($\approx 3{\cdot}8\,MPa\sqrt{m}$) and the basic levels K_{Ic}^{gb} and K_{Ic}^{L} ($1{\cdot}4$–$2{\cdot}5\,MPa\sqrt{m}$) is dissipation by crack branching and grain bridging as proposed first by Hübner & Jillek[41] and by Knehans & Steinbrech.[42]

—As noted previously in experimental work,[25] microcrack toughening is the dominating mechanism in ZTA explaining the 60% increase in toughness compared with Al_2O_3.

—Although transformation toughening is the most important dissipative mechanism in TZP, its contribution to the macroscopic toughness with about +30% is so small that it is only sufficient to balance the toughness decrease which is associated with microcracking described by $(1-\omega)$. Contrary to Al_2O_3 and ATC, in TZP with its fine grain size, crack branching should be unimportant: following Table 2, for zirconia $K_{Ic} \approx K_{Ic}^{gb} \approx K_{Ic}^{L}$—in good agreement with the estimation of dissipation mechanisms in Table 3 (assuming the dissipation-free level K_{Ic}^{0} in Y-TZP to be given by K_{Ic}^{gb} or by K_{Ic}^{L}).

4 Discussion

The incorporation of 20 μm large Al_2O_3 grains in TZP–C (Fig. 5) is associated with the introduction of

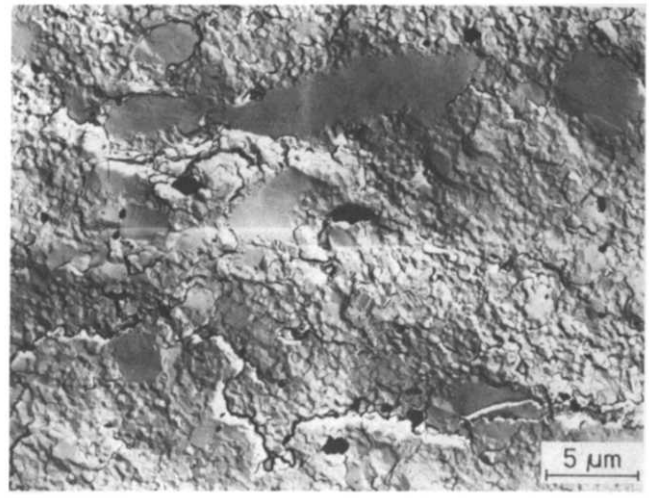

Fig. 5. Composite of four replica micrographs imaging the fracture surface of TZP–MC[b] (3 mol% Y_2O_3–ZrO_2 with 25 wt% of coarse Al_2O_3).

flaws due to (among other effects) differential sintering; resulting flaws are expected to approximate the Al_2O_3 grain size.[23] Further, following Table 2, Al_2O_3/Al_2O_3 interfaces should exhibit lower K_{Ic}^{gb} than ZrO_2/ZrO_2 boundaries, and this local heterogenization of K_{Ic}^{gb} in high alumina TZP/Al_2O_3 may provide additional microflaws generating cracking with all the possible useful or damaging consequences. However, at room temperature no detrimental effect of the coarse Al_2O_3 on the strength is observed. The conclusion is that both with such a high concentration of coarse Al_2O_3 and also at low contents of small Al_2O_3 grains (TZP–HF as well as pure Y-TZP with similar strength of about 1000 MPa) the macroscopic mechanical behaviour is not determined by small intrinsic flaws of the 0·6 μm TZP structure but, as suggested in Section 1, by more extended, at least about 20 μm, large defects produced extrinsically, e.g. by powder processing, sintering or grinding.

The microstructural observations and the data in Table 2 confirm the correspondence of microporosity within plain grain facets with the grain boundary toughness K_{Ic}^{gb} for transformation-free as well as for transforming ceramic microstructures. However, no simple correlation exists with the occurrence of amorphous grain boundary films, substantiating the idea of three independently working requirements for microporosity, as discussed in Section 1. Whereas in Y-TZP a continuous amorphous boundary phase prevents nucleation and growth of micropores by hindering the development of sufficiently high residual stresses, in ATC it is the absence of such glassy interfaces and the associated high boundary viscosity that produces the same microstructural result and enhances K_{Ic}^{gb}.

All of the examined ceramics reveal fracture-induced microcracking or crack branching well above the limit of significance but without a general correlation to K_{Ic}^{gb}. As demonstrated by TZP whose $\Delta C_{m\,ZrO_2}$ is higher than that of ZTA but with a decreased crack density, homogeneously distributed amorphous interfaces and a high degree of stress-induced transformation do not necessarily promote microcracking.

Instead there is some indication of a correlation between the crack density and the distribution of microflaws in agreement with the idea that isolated microcracks (separate from the macrocrack) are produced at the sites of such flaws due to the local stress concentration. Therefore the low degree of microcracking in TZP (compared with ZTA) is understood as a consequence of a high grain boundary strength promoted by a high grain boundary toughness *and* by the small size of glass-filled triple-point flaws.

In ZTA and Y-TZP microcrack toughening and transformation toughening are the dominating microprocesses that dissipate stored elastic strain energy on the scale of some grain sizes (Table 3). Whereas in ZTA the mechanism provides a relatively high toughness, in TZP it only balances the detrimental effect of microcrack damage. The reason is the high critical stress for the initiation of martensitic transformation in Y-TZP. Hence the macroscopic toughness of Y-TZP should be generated by, finally, the high basic level of K_{Ic}^{L}: for TZP the calculations (Section 3.3) resulted in $K_{Ic} \approx K_{Ic}^{0} \approx K_{Ic}^{gb} \approx K_{Ic}^{L}$. It is this exceptionally high K_{Ic}^{L}, probably due to some kind of energy dissipation mechanism within the grains as discussed by Michel *et al.*[36] and by Heuer *et al.*,[43] that produces the macroscopic toughness. Of course there is no direct influence of processes inside the grains on fracture because of the very low degree of transgranular spalling, but similar mechanisms will take place at grain surfaces, giving rise to an enhanced boundary toughness as long as no additional interface damage occurs.

As to ATC, the conclusions derived in Section 3.3 from Table 3 suggest a similar macroscopic toughness for ATC as for Al_2O_3, whereas the measurements (Table 2) reveal $K_{Ic}(ATC) \approx 1{\cdot}3 K_{Ic}(Al_2O_3)$ and give approximately the same ratio for the K_{Ic}^{gb}. Although at present no theoretical model predicts the quantitative influence of K_{Ic}^{gb} on K_{Ic}, it seems reasonable to expect the increased K_{Ic}^{gb} of ATC to be the reason for the improve macroscopic toughness. Therefore the macroscopic toughness of TZP and ATC has to be understood without energy dissipation above the scale of the grains. In both ceramics there is a perfect interface structure (Fig. 3) and a high K_{Ic}^{gb} that play the deciding role.

Then, comparing with the reference materials Al_2O_3 and ZTA, the final question is why with 'usual' extrinsic flaws both TZP and ATC exhibit an increase of the strength that is much more pronounced than that of their K_{Ic}. The idea that appeals most to the present authors is an *intrinsically* caused reduction of the growth of the *extrinsic* flaws, the original 'starting' size of which is always about 10–30 μm. Usually, on loading a ceramic part, such flaws grow subcritically along grain boundaries till they reach instability at a size of 50–150 μm, but in Y-TZP and ATC extremely high K_{Ic}^{gb} decrease the subcritical velocity by some orders of magnitude, and the result is a corresponding increase of the strength even at constant K_{Ic}.[5] Two recent observations substantiate this idea. Working on *R*-curves of Y-TZP, Anderson & Braun[44] found no influence of humidity and cross-head speed: no further reduction of an eventual subcritical growth was possible. For ATC preliminary experiments made in the laboratory of the present authors showed the usual $v \sim (K_I)^n$ relationship, but compared with Al_2O_3 sintered similarly in a reducing atmosphere the crack growth velocity v in ATC was about 4–7 orders of magnitude lower than in Al_2O_3.

Since strengthening by inherent reinforcement (increasing K_{Ic}^{gb}) appears to be associated with the production of micropore-free grain boundaries, the reduction of grain sizes will be a beneficial measure if microporosity is suppressed by reducing residual stresses under the condition of a homogeneously distributed amorphous phase: visco-elastic relaxation occurs the faster the smaller the grain size.[45] Of course the high-temperature strength is naturally restricted with amorphous interfaces, at least for a glass composition such as is common in TZP with coarse Al_2O_3 additions. As demonstrated by Table 2, it is the alternative way to suppress microporosity by increasing grain boundary viscosity (ATC) that gives a high strength not only at room temperature but also at 1000°C. A reduction of the grain size will be favourable here too, since in any structure this is associated with a smaller size of microscopic stress concentrators and, thereby, increased grain boundary strength. It should be remembered, however, that in transformation-free as in transforming ceramics with or without amorphous phases a decreasing grain size almost always reduces the energy dissipative mechanisms discussed in Section 3.3.

In addition to the original aims of this work, the results enable further insight into the nature of

microcracks that intersect the macroscopic fracture surfaces. In Section 3.1 it was suggested that the lack of a correlation between crack densities and K_{Ic}^{gb} occurs because close to the macrocrack tip the local stress concentration overcomes σ_f^{gb}. Whereas this probably remains true for Al_2O_3 and ZTA, the hypothesis must be questioned for ATC and TZP in the light of their high σ_f^{gb} (Table 2): evaluating the local stress at a distance r in front of a surface crack by $\sigma_I(r) = K_I/\sqrt{2\pi r}$,[46] with the maximum $K_I = K_{Ic} = 5\ MPa\sqrt{m}$, the local stress exceeds 5000 MPa at $r \leq 0{\cdot}3\ \mu m$. Regarding σ_f^{gb} and the grain sizes for ATC and TZP in Tables 1 and 2, it should be impossible to generate isolated microcracks by failure of individual interfaces separate from the macrocrack. Therefore the images of fracture surfaces used to determine the 'microcrack' densities (e.g. for Table 2) probably do not always show originally isolated microcracks that have linked up in a second stage: at least for TZP and ATC they are more likely to reveal traces of macrocrack branching and bridging, as discussed by Knehans & Steinbrech.[42] Nevertheless, the conclusion of an almost negligible contribution of microcrack toughening in both these materials remains correct.

The interdependence of the concentration of amorphous phases and grain size with the strength of Y-TZP needs further examination. It has been argued by Whalen *et al.*[47] that an increased SiO_2 content in Y-TZP favours Y_2O_3 segregation in grain boundaries, causing a destabilization of the tetragonal phase.[48] Table 1 supports these findings as to the *spontaneous* transformation in TZP/Al_2O_3 (cf. TZP–LC/MC) but rejects it as a generally working influence for the stress-induced transformation on fracture.

Further, following the results in Tables 1 and 2, at similar grain sizes similar high-strength Y-TZP can be produced with 0·15 as well as with 0·50 wt% SiO_2 (TZP–LC/MC); but with really equal grain sizes the higher strength was observed for the purer material. Hence no generally working description for the effect of SiO_2 under varying circumstances can be derived at present.

As to the grain size, in addition to the effect of $K_{Ic}^{gb} \approx K_{Ic}^{L}$, the macroscopic toughness of Y-TZP might be raised by making use of the 30% increase due to process (III) in Table 3 if microcrack damage can be avoided in spite of the high $\Delta C_{m\text{-}ZrO_2}$. In fact, Anderson & Braun[44] have reported increasing K_{Ic} with growing grain size (i.e. decreasing σ_{pc}) in Y-TZP.

Compared to Y-TZP, where Y_2O_3 reduces the grain growth[16] and stabilizes the tetragonal modification, stabilization with Ce gives a much higher toughness of 10–20 $MPa\sqrt{m}$ but with a modest strength of 600–800 MPa.[49] If the conclusions derived in the present work are correct, then the different strengths obtained with different stabilizers, such as Y, Ce, Mg and Ca, are caused first of all by different grain boundary structures due to different segregation, glass composition and stress relaxation (at different grain sizes), whereas a differing transformation behaviour may affect K_{Ic}. A comparative examination of grain boundary structures in differently stabilized TZP ceramics would be informative in this connection.

5 Conclusions

(1) Experiments with large Al_2O_3 grains (2–20 μm) within a fine-grained TZP matrix (0·6 μm) did not reveal any influence on the strength at room temperature. It is concluded that (a) the strength of this pressureless sintered Y-TZP is controlled by extrinsic flaws generated by powder processing, sintering and grinding, and that (b) the starting size of such flaws approximates at least to that of the largest of the added Al_2O_3 grains. Therefore it turns out that the small grain sizes in Y-TZP do not result in a direct, adequate reduction of the original flaw sizes that initiate the macroscopic fracture. The important consequence is that the high strength of these ceramics should be caused by a decreased difference between the original and the final flaw size developed on fracture, i.e. by a strong limitation of subcritical crack growth.

(2) Previous examinations of different alumina structures revealed an interdependence of improved grain boundary perfection and rising K_{Ic}^{gb}. Further experiments with Al_2O_3/TiC (ATC), the grain facets of which material are almost completely free of any amorphous phase and free of microdefects, give evidence that it is possible:

   (i) to raise K_{Ic}^{gb} to a level of 0·90–0·95K_{Ic}^{L} by eliminating micropores due to the elimination of amorphous grain boundary films,
   (ii) to raise by this means the macroscopic toughness K_{Ic}, and
   (iii) to increase the strength more than K_{Ic} by reducing subcritical crack growth as a consequence of (i).

   Of course the elimination of amorphous phases gives additional benefit at high temperatures.

(3) However, a high level of micromechanical grain boundary parameters does not necessarily require the elimination of amorphous phases: the comparison of the degrees of transformation and microcracking on fracture in Y-TZP and in ZTA gives reference for the increased grain boundary strength in the first material—associated (as well as in ATC) with an extreme perfection of grain boundaries. In Y-TZP the obvious cause is the high relaxation ability of the extremely fine-grained structure with its continuous amorphous grain boundary phase. Such interface structures are assumed to generate the high room-temperature strength in Y-TZP by a mechanism as proposed in conclusion (1). It is clear, however, that this concept does not work at high temperatures.

(4) Theoretical analyses of the experimental results demonstrate that the macroscopic toughness K_{Ic} in Y-TZP is—quite similarly to ATC—first of all dictated by the high level of grain boundary strength and toughness (and to a much smaller extent only by transformation toughening, which is the main mechanism of energy dissipation in this material).

(5) Hence an inherent reinforcement of ceramic microstructures with the objective of a direct impact on high strength is possible with two alternative concepts: (a) raising the high-temperature viscosity of grain boundary regions by almost complete elimination of amorphous phases on grain boundary facets, and (b) by enhancing the relaxation efficiency with a continuous thin glassy film in an extremely fine-grained microstructure. Discontinuously distributed amorphous phases are regarded as especially unfavourable in this respect because they provide increased possibilities for the residual stress-assisted development of grain boundary micropores.

Acknowledgements

The experimental work on TZP was supported by the Federal Minister of Research and Technology of the Federal Republic of Germany under Contract No. 33 L 101400. The authors are glad to acknowledge the cooperation in the TEM structural analysis of Dr J. Woltersdorf and Dr E. Pippel, who are with the Max Planck Institute of Microstructure Physics at Halle/Saale and who supplied the HREM results discussed in this paper. The contributions of Dr J. Henke and Dr J. Edelmann, who were responsible for the X-rays and electron microscopical analyses at the Dresden institute, are also gratefully acknowledged.

References

1. Fischmeister, H. F., Structure and properties of high angle boundaries. *J. de Phys. Colloque C4/Suppl.*, **46** (1985) 3–21.
2. Rühle, M., Comparisons between observed and computed grain boundary structures and energies in ceramics. *J. de Phys. Colloque C4/Suppl.*, **46** (1985) 281–92.
3. Suga, T. & Elssner, G., Determination of fracture energy and the fracture resistance of interfaces. *J. de Phys. Colloque C4/Suppl.*, **46** (1985) 657–63.
4. Krell, A., Woltersdorf, J., Pippel, E. & Schulze, D., On grain boundary strength in sintered Al_2O_3. *Phil. Mag. A*, **51** (1985) 765–76.
5. Krell, A. & Pompe, W., The influence of subcritical crack growth on the strength of ceramics. *Mater. Sci. Eng.*, **89** (1987) 161–8.
6. Krell, A., Pippel, E. & Woltersdorf, J., On crack-propagation related phenomena in $Al_2O_3+ZrO_2$ and Al_2O_3 sintered in air and in hydrogen. *Phil. Mag. A*, **53** (1986) L11–6.
7. Pippel, E. & Woltersdorf, J., High-voltage and high-resolution electron microscopy studies of interfaces in zirconia-toughened alumina. *Phil. Mag. A*, **56** (1987) 595–613.
8. Pompe, W., Bahr, H.-A., Werdin, S. & Balke, H., Non-stationary nucleation of micropores at grain boundaries of engineering ceramics. In *Proc. 9th Int. Congress on Powder Metall.*, Zentralinstitut für Festkörperphysik und Werkstofforschung, Dresden, Vol. 3, 1989, pp. 227–39.
9. Pompe, W. & Bahr, H.-A., Verbesserung der mechanischen Eigenschaften von Keramiken durch gezielte Eigenspannungsentwicklung. *Silikattechnik*, **38** (1987) 97–102.
10. Krell, A. & Pompe, W., Grain boundary microdamage due to visco-elastic relaxation of residual stresses in alumina ceramics. *Phys. Stat. Sol. (A)*, **111** (1989) 109–17.
11. Krell, A. & Grigorjew, O. N., Gefügeeigenspannungen und Mikroporosität in Oxidkeramik. *Sprechsaal*, **123** (1990) 1012–15.
12. Kobayashi, K. & Masaki, T., Toughened zirconia. *J. Japan. Ceram. Soc.*, **17** (1982) 427.
13. Masaki, T., Mechanical properties of toughened ZrO_2–Y_2O_3 ceramics. *J. Am. Ceram. Soc.*, **69** (1986) 638–40.
14. Tsukuma, K., Ueda, K. & Shimada, M., Strength and fracture toughness of isostatically hot-pressed composites of Al_2O_3 and Y_2O_3-partially stabilized ZrO_2. *J. Am. Ceram. Soc.*, **68** (1985) C4–5.
15. Rajendran, S., Swain, M. V. & Rossel, H. J., Mechanical properties and microstructures of co-precipitation derived tetragonal Y_2O_3–ZrO_2–Al_2O_3 composites. *J. Mater. Sci.*, **23** (1988) 1805–12.
16. Lange, F. F., Controlling grain growth. In *Annual Report No. 1 for the Period 1.9.85–31.8.86*, ed. F. F. Lange & D. B. Marshall. Rockwell Int. Science Center, Thousand Oaks, California, 1986, Chapter 6.0.
17. Hoshi, Y., Obitu, M., Awano, M. & Takagi, H., Al_2O_3–PSZ ceramics with high flexural strength and high fracture toughness. *Interceram*, **39** (1990) 24–6.
18. Wang, J., Rainforth, M. & Stevens, R., The grain size dependence of the mechanical properties in TZP ceramics. *Trans. Brit. Ceram. Soc.*, **88** (1989) 1–6.
19. Riedel, G., Bürger, W., Chýlek, S. & Vrbacký, I., Feinkristalline, niedrigsinternde Korundkeramik. *Silicates Ind.*, **54** (1989) 29–35.

20. Hecht, N. L., Jang, S. D. & McCullum, D. E., Environmental effect on toughened zirconia ceramics. In *Advances in Ceramics*, Vol. 24A (Zirconia III), ed. S. Somiya, N. Yamamoto & H. Yanagida. The American Ceramic Society, OH, 1988, pp. 133–44.
21. Hayashi, K., High strength alumina sintered body and process for preparation thereof. European Patent Application EP-321955, 1989.
22. Shin, D. W., Orr, K. K. & Schubert, H., Microstructure–mechanical property relationship in hot-isostatically pressed alumina and zirconia-toughened alumina. *J. Am. Ceram. Soc.*, **73** (1990) 1181–8.
23. Tuan, W. H. & Brook, R. J., Sintering of heterogeneous ceramic compacts. Part 2: ZrO_2–Al_2O_3. *J. Mater. Sci.*, **24** (1989) 1953–8.
24. Rühle, M. & Heuer, A. H., The martensitic reaction in t-ZrO_2. In *Advances in Ceramics*, Vol. 12 (Zirconia II), ed. N. Claussen, M. Rühle & A. H. Heuer. The American Ceramic Society, OH, 1984, pp. 14–32.
25. Krell, A., Blank, P. & Weiss, T., Influence of microcracking and homogeneity on the mechanical behaviour of (Al_2O_3 + ZrO_2) ceramics. *J. Mater. Sci.*, **22** (1987) 3304–8.
26. Cotterell, B. & Rice, J. R., Slightly curved or kinked cracks. *Int. J. Fracture*, **16** (1980) 155–69.
27. Krell, A. & Schulze, D., Quantitative Untersuchungen von Mikrorißstrukturen in gesintertem Aluminiumoxid. *Silikattechnik*, **36** (1985) 294–6.
28. Chantikul, P., Anstis, G. R., Lawn, B. R. & Marshall, D. B., A critical evaluation of indentation techniques for measuring fracture toughness. II: Strength method. *J. Am. Ceram. Soc.*, **64** (1981) 539–43.
29. Lawn, B. R., Evans, A. G. & Marshall, D. B., Elastic–plastic indentation damage in ceramics: the median/radial crack system. *J. Am. Ceram. Soc.*, **63** (1980) 574–81.
30. Pippel, E. & Woltersdorf, J., Electron microscopy of TiC containing alumina ceramics. *Phys. Stat. Sol. (A)*, **116** (1989) 165–78.
31. Krell, A. & Schulze, D., ⟨1210⟩-Zone fracture anisotropy of sapphire. *Phys. Stat. Sol. (A)*, **52** (1979) K45–8.
32. Breval, E., Fracture and plastic deformation of titanium carbide at room temperature. *Scand. J. Metall.*, **10** (1981) 51–4.
33. Baldoni, J. G., Buljan, S. T. & Sarin, V. K., Particulate titanium carbide–ceramic matrix composites. In *Science of Hard Materials*, ed. E. A. Almond, C. A. Brookes & R. Warren. Adam Hilger Ltd, Bristol, 1986, pp. 427–38.
34. Warren, R., Measurement of the fracture properties of brittle solids by Hertzian indentation. *Acta Metall.*, **26** (1978) 1759–69.
35. Ingel, R. P., Lewis, D., Bender, B. A. & Rice, R. W., Temperature dependence of strength and fracture toughness of ZrO_2 single crystals. *J. Am. Ceram. Soc.*, **65** (1982) C150–2.
36. Michel, D., Mazerolles, L. & Perez y Jorba, M., Fracture of metastable tetragonal zirconia crystals. *J. Mater. Sci.*, **18** (1983) 2618–28.
37. Pompe, W. & Kreher, W., Theoretical approach to energy-dissipative mechanisms in zirconia and other ceramics. In *Advances in Ceramics*, Vol. 12 (Zirconia II), ed. N. Claussen, M. Rühle & A. H. Heuer. The American Ceramic Society, OH, 1984, pp. 283–92.
38. Kreher, W., Report No. 85/1/05, Zentralinstitut für Festkörperphysik und Werkstofforschung, Dresden, 1985.
39. Evans, A. G. & Faber, K. T., Crack-growth resistance of microcracking brittle materials. *J. Am. Ceram. Soc.*, **67** (1984) 255–60.
40. Koyama, T. & Nishiyama, A., High-strength Al_2O_3–Ti(C,N) ceramics by HIP and cutting performance. Paper presented at the *7th CIMTEC Congress*, 24–30 June 1990, Montecatini Terme, Italy.
41. Hübner, H. & Jillek, W., Subcritical crack extension and crack resistance in polycrystalline alumina. *J. Mater. Sci.*, **12** (1977) 117–25.
42. Knehans, R. & Steinbrech, R., Memory effect of crack resistance during slow crack growth in notched Al_2O_3 bend specimens. *J. Mater. Sci. Lett.*, **1** (1982) 327–9.
43. Heuer, A. H., Chaim, R. & Lanteri, V., The displacive cubic–tetragonal transformation in ZrO_2 alloys. *Acta Metall.*, **35** (1987) 661–6.
44. Anderson, R. M. & Braun, L. M., Technique for the *R*-curve determination of Y-TZP using indentation-produced flaws. *J. Am. Ceram. Soc.*, **73** (1990) 3059–62.
45. Blendell, J. E. & Coble, R. L., Measurement of stress due to thermal expansion anisotropy in Al_2O_3. *J. Am. Ceram. Soc.*, **65** (1982) 174–8.
46. Irwin, G. R., Analysis of stresses and strains near the end of a crack traversing a plate. *J. Appl. Mech.*, **24** (1957) 361–4.
47. Whalen, P. J., Reidinger, F., Correale, S. T. & Marti, J., Yttria migration in Y-TZP during high-temperature annealing. *J. Mater. Sci.*, **22** (1987) 4465–9.
48. Schubert, H., Claussen, N. & Rühle, M., Einfluß der intergranularen Glasphase auf die Umwandlungsfähigkeit von TZP. In *Techn. Keram. Werkstoffe*, ed. J. Kriegesmann. Deutscher Wirtschaftsdienst, Köln, 1990, Part 5.1.3.1, pp. 1–10.
49. Tsukuma, K. & Shimada, M., Strength, fracture toughness and Vickers hardness of CeO_2-stabilized tetragonal ZrO_2 polycrystals. *J. Mater. Sci.*, **20** (1985) 1178–84.